Princeton Plasma Physics Laboratory

PPPL-4236

PPPL-4236

Nonlocal Properties of Gyrokinetic Turbulence and Role of E x B Flow Shear

W.X. Wang, T.S. Hahm, W.W. Lee,
G. Rewoldt, J. Manickam, and W.M. Tang

(Preprint)
May 2007

PPPL
PRINCETON PLASMA
PHYSICS LABORATORY

Prepared for the U.S. Department of Energy under Contract DE-AC02-76CH03073.

Princeton Plasma Physics Laboratory
Report Disclaimers

Full Legal Disclaimer

Trademark Disclaimer

PPPL Report Availability

Princeton Plasma Physics Laboratory:

http://www.pppl.gov/techreports.cfm

Office of Scientific and Technical Information (OSTI):

http://www.osti.gov/bridge

Related Links:

U.S. Department of Energy

Office of Scientific and Technical Information

Fusion Links

Nonlocal properties of gyrokinetic turbulence and role of $\mathbf{E} \times \mathbf{B}$ flow shear

W. X. Wang,* T. S. Hahm, W. W. Lee, G. Rewoldt, J. Manickam, and W. M. Tang

Princeton University, Plasma Physics Laboratory,

P.O. Box 451, Princeton, NJ 08543

Abstract

The nonlocal physics associated with turbulent transport is investigated using global gyrokinetic simulations with realistic parameters in shaped tokamak plasmas. We focus our studies on the turbulence spreading through a transport barrier characterized by an equilibrium $\mathbf{E} \times \mathbf{B}$ shear layer. It is found that an $\mathbf{E} \times \mathbf{B}$ shear layer with an experimentally relevant level of the shearing rate can significantly reduce, and sometimes even block, turbulence spreading by reducing the spreading extent and speed. This feature represents a new aspect of transport barrier dynamics. The key quantity in this process is identified as the local maximum shearing rate $|\omega_E^{max}|$, rather than the amplitude of the radial electric field. Our simulation studies also extend to radially local physics with respect to the saturation of the ion temperature gradient (ITG) instability, and show that the nonlinear toroidal couplings are the dominant k-space activity in the ITG dynamics, which cause energy transfer to longer wavelength damped modes, forming a down-shifted toroidal spectrum in the fully developed turbulence regime.

PACS numbers: 52.65Tt, 52.65Rr, 52.25Fi

I. INTRODUCTION

Tokamak experiments often show evidence that nonlocal dependence exists in plasma transport. For collision-driven neoclassical transport, the nonlocality is introduced when the particle drift orbit size is not small compared to the plasma equilibrium scale length and/or the plasma local minor radius.[1] For turbulence-driven transport, it is believe that the nonlocality is caused by the radial propagation of the fluctuations,[2] or so-called turbulence spreading. Understanding turbulence spreading is one important step toward quantitatively predicting turbulent transport in burning plasmas, and it is proposed as an explanation for turbulent transport scaling with machine size.[3–6] In this work, the nonlocal physics associated with turbulent transport is investigated using a newly developed simulation capability. Our global simulations, based on a generalized gyrokinetic particle model, incorporate the comprehensive influence of non-circular cross section, realistic plasma profiles, plasma rotation, neoclassical (equilibrium) electric fields, and Coulomb collisions,[7] and therefore can effectively address the following important, experimentally relevant issues.

Our simulations of ion temperature gradient (ITG) turbulence are carried out for shaped toroidal plasmas roughly based on DIII-D geometry and parameters. By a series of carefully designed numerical experiments, both with and without nonlinearity, and both with and without zonal flows, we demonstrate that turbulence spreading is quite a generic phenomenon, but exhibits different characteristics depending on the underlying dynamics. It is believe that equilibrium $\mathbf{E} \times \mathbf{B}$ shear flows play an important role in controlling the turbulence level and the associated transport locally. While radially local comparisons between the $\mathbf{E} \times \mathbf{B}$ shearing rate, ω_E,[8] and the linear growth rate of an instability[9] have served as a useful rule of thumb for the transport barrier formation condition in many experiments,[10] some experiments report the existence of density fluctuations and anomalous heat transport in the region of almost flat density and temperature profiles, inside the location of the internal transport barrier.[11] Motivated by this, we focus our studies on the turbulence spreading through a transport barrier characterized by an $\mathbf{E} \times \mathbf{B}$ shear layer. These studies can provide interesting new insight into transport barrier physics. We perform a series of numerical experiments by placing a radial electric field well, with varying strength, next to the region where the ITG instability is linearly unstable. It is found that an $\mathbf{E} \times \mathbf{B}$ shear layer with an experimentally relevant level of the shearing rate can significantly reduce, and

sometimes even block, turbulence spreading by reducing the spreading extent and speed. From the spatio-temporal evolution of the turbulence propagation front, we find that the spreading slows down significantly in the region of higher $|\omega_E|$, rather than at the bottom of the E_r well. Therefore, we conclude that the $\mathbf{E} \times \mathbf{B}$ shearing rate is the key local quantity in slowing down, and possibly blocking, turbulence spreading.

Local physics and nonlocal physics are two aspects that determine the global turbulence fluctuation level and associated transport. Our simulations are also extended to study nonlinear toroidal spectral transfer in ITG turbulence. It is observed that nonlinear toroidal couplings as a fundamental local process are strongly correlated with ITG saturation, and responsible for the formation of a down-shifted toroidal spectrum in the fully developed turbulence regime.

This paper is organized as follows. In Sec. II, the turbulence spreading process observed from our global simulations is described, and the characteristics of linear/nonlinear spreadings and the effect of zonal flows are discussed. The role of an equilibrium $\mathbf{E} \times \mathbf{B}$ shear layer in turbulence spreading is addressed in Sec. III. The nonlinear toroidal spectral cascade behavior in ITG dynamics is reported in Sec. IV, followed by discussion and conclusions in Sec. V.

II. DYNAMICS OF TURBULENCE SPREADING AND EFFECT OF ZONAL FLOWS

If turbulence can spread or propagate radially, the level of fluctuations at one radial position can depend on the drive of instabilities located elsewhere. This results in transport nonlocality. Indeed, a number of global transport phenomena can occur as a direct consequence of turbulence spreading. While turbulence spreading has been widely observed in direct numerical simulations since 1994,[2] the recent high level of interest has occured as this has been proposed as a physics mechanism[4] responsible for the deviation of transport scaling from gyroBohm scaling at moderate system sizes. A nonlocal mechanism is necessary to explain this deviation, since local turbulence characteristics compatible with gyroBohm scaling are observed in global nonlinear gyrokinetic simulations of ITG turbulence.[3]

The role of turbulence spreading in breaking the gyroBohm scaling of transport has been further confirmed from a different gyrokinetic simulation[6] and from different theo-

retical considerations.[12] More recent applications of turbulence spreading include edge-core coupling,[13] turbulence tunneling through a linearly stable gap,[14] the role of zonal flows,[15–17] applications to reversed shear plasmas,[18] the particle transport problem,[19] and extensions to a multi-field model.[17]

To enhance our understanding of the physics mechanisms behind turbulence spreading, we have performed a series of numerical experiments using the new capabilities of the GTC-S code[7] which is based on a generalized gyrokinetic particle simulation model of tokamak geometry, and has been developed using the GTC architecture.[3,5] An overall picture of global turbulence development due to turbulence spreading is illustrated in Fig. 8 of our previous paper, Ref. 7, which shows the spatio-temporal evolution of the flux-surface averaged turbulence intensity and contour plots of the electric potential at three different times. This is for an ITG simulation for geometry and plasma parameters which are roughly based on DIII-D. The unstable region for the ITG mode in this simulation is $0.42 < r < 0.76$ (where r in units of the plasma minor radius a). At an early time before nonlinear saturation, the turbulence is driven initially in the linearly unstable region, generating radially elongated toroidal eigenmodes (streamers),[20] with small extensions into the two adjacent linearly stable zones via linear toroidal coupling. Later on, the turbulence eddies are broken up by the self-generated $\mathbf{E} \times \mathbf{B}$ shearing flows (zonal flows) during the nonlinear saturation phase. A major radial expansion of the fluctuations, associated with nonlinear wave couplings, immediately follows. The fluctuations spread in both the inward and outward radial directions into the linearly stable regions, eventually leading to radially global turbulence. The fluctuation levels in the stable regions are comparable to that in the original unstable region, which causes enhanced ion energy transport in the stable regions. Transport nonlocality is established by the coupling between the linearly stable and unstable regions.

For the same simulation, the time evolution of the turbulence intensity at two radii, one in the unstable region and the other in a stable region, is presented in Fig. 1. Here, time is in units of L_{Ti}/v_{thi}, where L_{Ti} is the ion temperature gradient scale length and v_{thi} is the ion thermal velocity. The spreading process is shown to have two phases. The first phase is a very small linear spreading which occurs before the saturation of the original instability. Later on, a major and fast spreading takes over after the saturation of the linear instability, which radially extends the fluctuations into the linearly stable zones.

It is important to note that during the turbulence spreading in our simulation, the profile

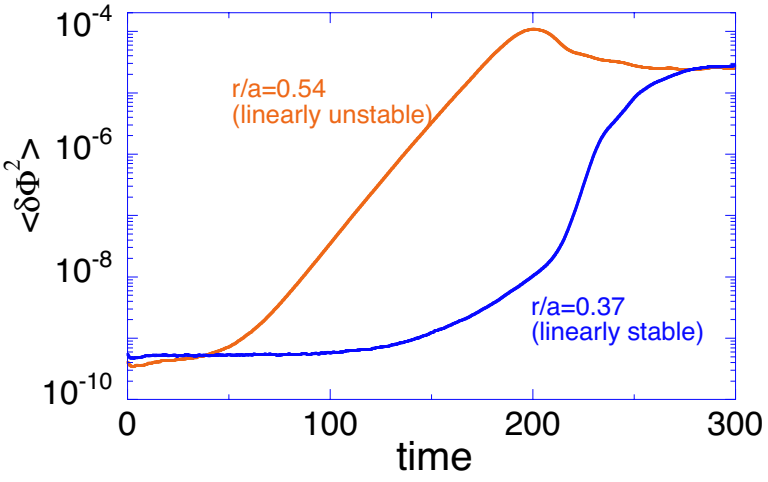

FIG. 1: Time evolution of the intensity at two radii, from a simulation of a shaped plasma with typical DIII-D parameters

relaxation is negligible. Therefore, the spreading is not a consequence of changes in the linear stability. As we described in Ref. 7, the **k**-spectra in the linearly stable regions are significantly different from those of the linear eigenmodes in the unstable region, having a substantial down-shift in k_θ.

As an example of mesoscale phenomena[21,22] which occur on scales larger than an eddy size but smaller than the system size, turbulence spreading has been widely observed in previous simulations in both toroidal geometry[23] and in the absence of toroidal coupling,[24,25] and both with[5] and without[26] zonal flows. As for nonlinear spreading, both three wave couplings[4,14,17] and nonlinear interactions between drift waves and zonal flows in toroidal geometry[12] have been proposed as underlying dynamics. To identify the relative roles of the linear toroidal mode coupling, nonlinear mode coupling, and self-generated zonal flows, we have carried out a series of numerical experiments to examine the properties of turbulence spreading associated with different mechanisms. In the absence of nonlinear mode coupling, as shown in Fig. 2-a, convective spreading occurs due to the linear toroidal mode coupling. This result is in agreement with a previous theory prediction by Garbet.[2] The convective spreading observed in this linear simulation is characterized by a constant front propagation velocity $V_s \simeq (\rho_i/R)C_s$, which is also independent of the turbulence intensity. Here ρ_i is the ion gyroradius, R is the major radius of the toroidal plasma and C_s is the sound speed.

As we turn on the nonlinearity, but with zonal flows artificially suppressed, the temporal

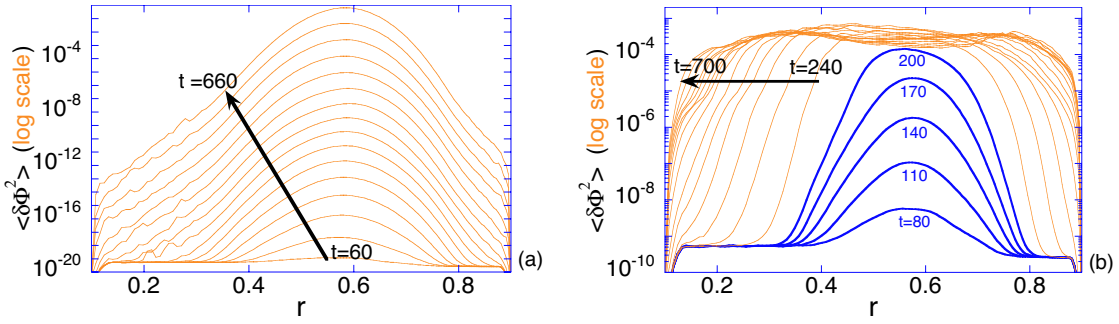

FIG. 2: Spatio-temporal evolution of turbulence intensity: (a) linear simulation with all modes and (b) nonlinear simulation without zonal flows.

behavior of the spreading becomes more complex, as shown in Fig. 2-b. First, a diffusive nature is additionally introduced into the spreading process by nonlinear mode couplings. The turbulence spreading is faster than that in the linear simulation. The front propagation velocity appears to be "convective" in the linearly unstable zone in agreement with the Fisher-Kolmogorov solution.[14] As the front approaches the region of weaker linear drive, it slows down and the propagation can be described as "diffusive" or "sub-diffusive".[4] The turbulence can spread all way to the boundaries of the simulation domain as the damping is not sufficiently strong.

Finally, the fluctuation envelope evolution, from simulations with the self-generated zonal flows, is plotted in Fig. 8-a of Ref. 7. The principle effect of zonal flows is to reduce the intensity of fluctuations, approximately by a factor of 10. Consequently, the spreading velocity is reduced as well. It is important to note that while zonal flows play a crucial role in determining the saturation value of the fluctuation intensity, there are other channels of nonlinear mode coupling which can saturate fluctuations even in the absence of zonal flows (this is shown in the simulation of Fig. 2-a, and associated nonlinear energy cascading will be addressed in Sec. IV). Therefore, it is hard to isolate the possible role of zonal flows in enhancing turbulence spreading, which has been predicted from an extension of the 4-wave theory[12,15] in which only the zonal flow mediated nonlinear interaction is kept. At least for the cases we have simulated, zonal flow induced enhancement of turbulence spreading has not been observed. A related theoretical discussion can be found in Gurcan et al.[17]

To elaborate our description of turbulence spreading dynamics in a more quantitative fashion, we perform the following analysis of the simulation data. We measure the turbulence

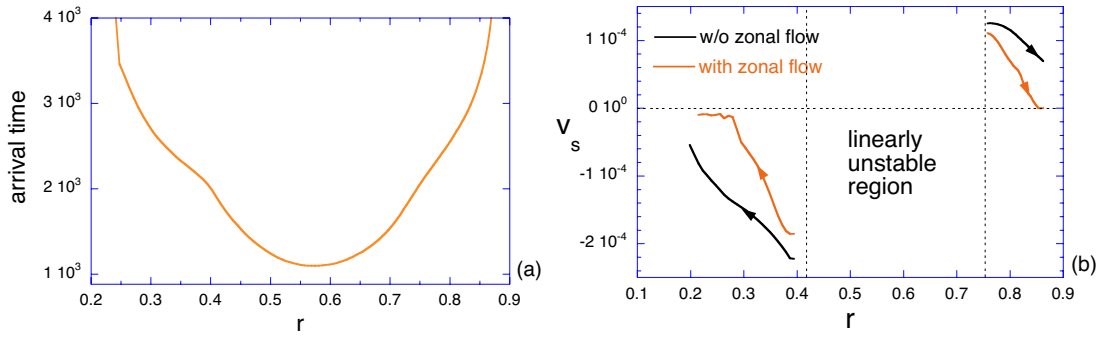

FIG. 3: (a) Arrival time of turbulence propagation front at different radii and (b) turbulence propagation velocity (positive and negative velocities indicate outward and inward propagation respectively.)

propagation velocity at each radius by recording the time at which the fluctuation front of a specified turbulence intensity passes through that point. The turbulence intensity used for the measurement is $\langle \delta\Phi^2 \rangle = 10^{-6}$. After recording the arrival time of the turbulence propagation front as a function of radius, which is shown in Fig. 3-a, we obtained the turbulence propagation velocity by taking a time derivative, which is plotted in Fig. 3-b. It is observed that the turbulence propagation becomes slower as fluctuations propagate away from the linearly unstable region. Moreover, in the presence of self-generated zonal flows, the propagation velocity is significantly reduced. Correspondingly, turbulence fluctuations are less expanded.

Following the concept used in describing the diffusive property of particle random motion, we further define the radial extent of the fluctuation envelope due to spreading using the following expression:

$$\overline{|\Delta r|^2} \equiv \frac{\int_{r_1}^{r_c} d^3x (r - r_c)^2 |\delta\Phi|^2}{\int_{r_1}^{r_c} d^3x |\delta\Phi|^2}, \tag{1}$$

where the spatial integral covers the linearly stable region from the inner boundary of the simulation domain ($r_1 = 0.1$ for this simulation) to the point where the linear growth rate vanishes ($r_c = 0.42$). The resulting displacement $(\overline{|\Delta r|^2})^{1/2}$ is also a quantitative measure of effective turbulence spreading. The results for $(\overline{|\Delta r|^2})^{1/2}$ vs time are presented in Fig. 4. First, this clearly shows that most of the turbulence spreading starts at about $t = 200$, right after the local nonlinear saturation of the ITG instability. Second, a qualitative distinction

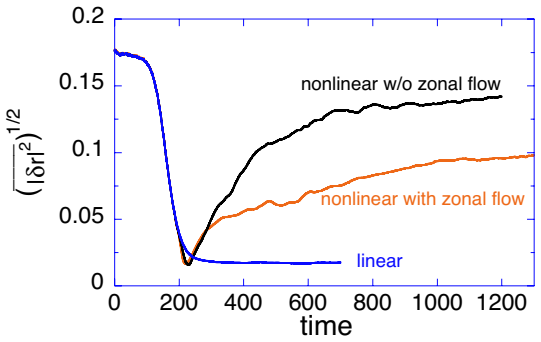

FIG. 4: Displacement of turbulence fluctuations vs time during turbulence spreading process.

between linear spreading and nonlinear spreading is clearly illustrated. In the linear simulation, convective turbulence propagation uniformly raises the fluctuations, as shown in Fig. 2-a, with approximately equal rates in the linearly stable regions. Correspondingly, it does not increase the effective turbulence extent as measured by the quantity $(\overline{|\Delta r|^2})^{1/2}$. In contrast, nonlinear spreading exhibits a partially diffusive nature, which leads to the expansion of the fluctuations. Both simulations with and without zonal flows show a gradual transition from convective to diffusive (and possibly sub-diffusive) propagation. In the presence of self-generated zonal flows, the effective spreading extent is significantly reduced, which is consistent with the reduction of the spreading velocity (as illustrated in Fig. 3-b). Finally, we note that the initial high level of $(\overline{|\Delta r|^2})^{1/2}$ is due to the spatially-uniform initial loading of small random fluctuations, which are not turbulence generated by the plasmas. Therefore, only the evolution after $t = 200$ is physically relevant.

III. TURBULENCE PROPAGATION THROUGH A TRANSPORT BARRIER – THE ROLE OF EQUILIBRIUM $\mathbf{E} \times \mathbf{B}$ FLOW SHEAR

As we discussed before, turbulence spreading appears quite generic. This sounds like a bad message for us. Indeed, recent experiments have shown evidence of turbulence spreading. For example, in JT-60U reversed shear plasmas, reflectometry measurements clearly show the existence of turbulence in the region inside internal transport barrier, where profiles are flat, and the microinstabilities are stable (as shown in Fig. 6 of Ref. 11). On the other hand, some experiments have observed ion thermal transport inside an internal transport barrier which is at a neoclassical level. In general, a transport barrier is characterized by a narrow $\mathbf{E}\times\mathbf{B}$ shear

flow layer associated with a steep pressure gradient and/or plasma rotation. It is believed that a significant $\mathbf{E} \times \mathbf{B}$ shear flow can suppress local turbulence by reducing the fluctuation amplitude, and sometimes entirely stabilizing the linear instability. An outstanding issue associated with transport barrier physics is: in additional to the quenching effect on local instability, can an $\mathbf{E} \times \mathbf{B}$ shear layer prevent turbulence from penetrating? To address this problem, we performed a number of numerical experiments using the aforementioned GTC-S code. A model $\mathbf{E} \times \mathbf{B}$ layer is placed next to the linearly unstable zone, as shown in the lower panel of Fig. 5, to represent a transport barrier. Here, we use an electric field well of following form:

$$\frac{d\Phi_0}{dr} = -E_0 \exp[-(\frac{r - r_c}{\Delta r})^2], \tag{2}$$

which is centered at radius $r_c = 0.35$. We vary the $\mathbf{E} \times \mathbf{B}$ shearing rate by changing the depth E_0. The shearing rate is defined by[8]

$$\omega_E = \frac{R^2 B_p^2}{B} \frac{\partial}{\partial \Psi_p} (\frac{E_r}{R B_p}), \tag{3}$$

where B and B_p are the total and poloidal magnetic field strengths, and Ψ_p is the poloidal magnetic flux.

Three numerical experiments with different $\mathbf{E} \times \mathbf{B}$ shearing rates are carried out. The radial profiles of turbulence intensity $\langle \delta\Phi^2 \rangle$ are plotted and compared in the upper panel of Fig. 5, which shows that the extent of the turbulence spreading decreases with increasing $\mathbf{E} \times \mathbf{B}$ shear. In the case of no $\mathbf{E} \times \mathbf{B}$ shear layer ($E_0 = 0$), as shown before, turbulence spreads widely to fill up a large area of the stable zones in both directions. The radial width of the turbulence fluctuation extent in the inward direction is about $25\rho_i$. As a consequence, significant heat transport is driven not only in the ITG source region, but is also observed all the way to a radial location $25\rho_i$ inside the source region. As a moderate radial electric field well is installed ($E_0 = 1$), with a maximum $\mathbf{E} \times \mathbf{B}$ shearing rate $\omega_E^{max} = 0.13 C_s/a$, it is observed that the inward spreading is partially blocked. In this case, the radial width of the fluctuation extent is reduced to about $12\rho_i$. As the applied E_r well becomes deeper and deeper, the blocking effect on the turbulence propagation becomes stronger and stronger. As illustrated in Fig. 5, the inward spreading is almost completed blocked for $\omega_E^{max} = 0.26 C_s/a$ ($E_0 = 2$). Correspondingly, a turbulence free or less turbulent plasma is obtained, which is decoupled from the turbulent plasma further out. This is clearly illustrated by the contour plots of the electric potential fluctuations, in Fig. 6. On the other hand, the turbulence

level is not increased in the ITG source region as inward spreading is blocked, and outward spreading is not affected. This indicates that the role of $\mathbf{E} \times \mathbf{B}$ shearing layer as a "barrier" for turbulence spreading is through a turbulence damping mechanism rather than through reflection of turbulence back to the source region. A shear layer not only reduces turbulence spreading extension, but also slows down the spreading.

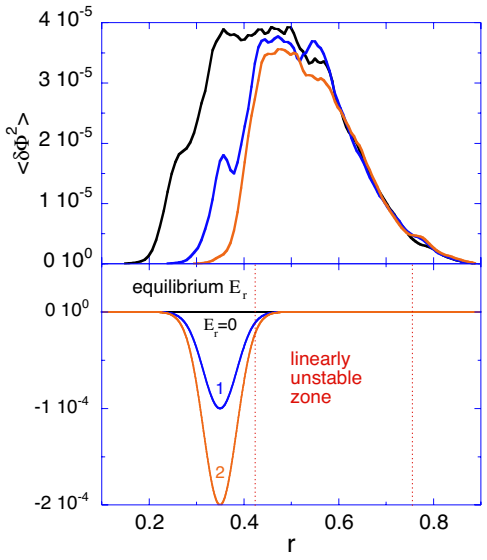

FIG. 5: The radial extent of turbulence spreading (of steady state fluctuation intensity) (upper panel) for three E_r wells (lower panel) located next to the unstable ITG source region.

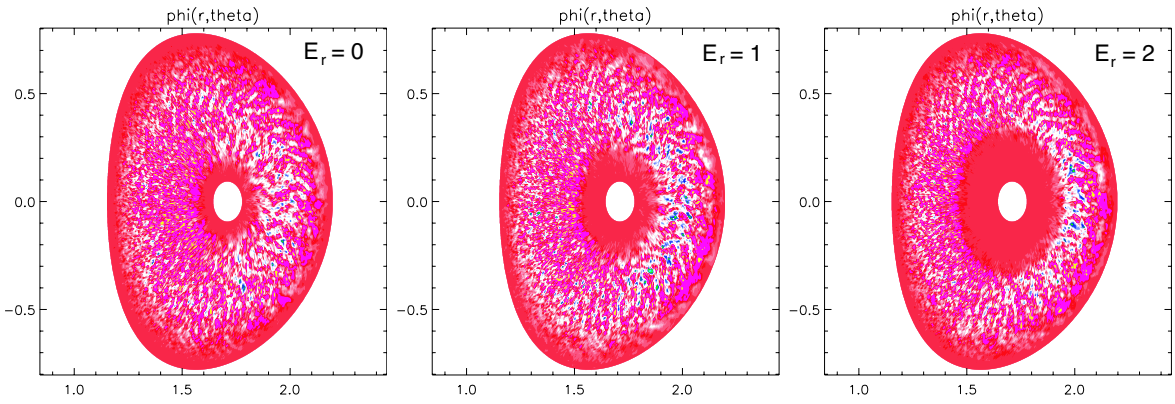

FIG. 6: Three corresponding contour plots of electric potential fluctuations at a poloidal plane, for simulations of Fig. 5.

Next, we attempt to clarify what elements play a key role in blocking the turbulence spreading. It is found that it is not E_r itself, but the $\mathbf{E} \times \mathbf{B}$ shear, which is the key to the

control of turbulence spreading. We examine the spatial-temporal evolution of turbulence front propagation which is presented in Fig. 7-a. For the electric field well used in the simulation, there are two peaks in the $\mathbf{E} \times \mathbf{B}$ shearing rate, located at around $r = 0.38$ and $r = 0.32$. As turbulence propagates from the unstable region (which is on the right in Fig. 7), entering into the $\mathbf{E} \times \mathbf{B}$ shear layer in the linearly stable region, the turbulence propagation front meets the first peak of ω_E^{max} at around $r = 0.38$. The propagation velocity significantly slows down, along with a reduction of the turbulence intensity. However, the first peak of $\mathbf{E} \times \mathbf{B}$ shear is not strong enough to completely block turbulence spreading. Once the turbulence propagation has passed through the first peak, the propagation becomes faster again in the region where E_r itself peaks while ω_E has a minimum. The turbulence keeps propagating until it reaches the second peak of the $\mathbf{E} \times \mathbf{B}$ shear at $r = 0.32$, which finally stops the turbulence spreading.

The same result is illustrated in Fig. 7-b in a more quantitative fashion, which shows the arrival time of the turbulence propagation front at different radii. The front propagation velocity is given by the time derivative of the curve, dr/dt, which is roughly denoted by the dotted lines. As one can see, the fluctuation front propagation slows down significantly when it crosses regions of the local maximum of the $\mathbf{E} \times \mathbf{B}$ shearing rate. This result clearly shows the critical role of the local maximum $\mathbf{E} \times \mathbf{B}$ shearing rate. It indicates that the role of the $\mathbf{E} \times \mathbf{B}$ shear layer in the control of turbulence spreading is through turbulence dissipation by shearing flows. Generally, the fluctuation level in a linearly stable region due to turbulence spreading is determined by the competition among radially inward turbulence flow coming from the remote instability source region, local dissipation, and radially outward turbulence flow to the next stable region. The overall spatio-temporal evolution of front propagation observed in the simulations is qualitatively consistent with the fact that the front propagation speed increases with the fluctuation intensity, and the fact that the $\mathbf{E} \times \mathbf{B}$ shear (not E_r) reduces the fluctuation intensity locally.

Based on a previous theory,[4] the nonlinear diffusion will cause a front to propagate in radius. In the absence of dissipation, the front will propagate indefinitely with its shape being maintained. The front propagation stops when the radial flux due to propagation is balanced by dissipation. We can estimate the extent of turbulence spreading into the linearly stable zone by equating the time required for the front to propagate a distance Δ to the inverse of the linear damping rate, which increases with radius. We have obtained a simple formula

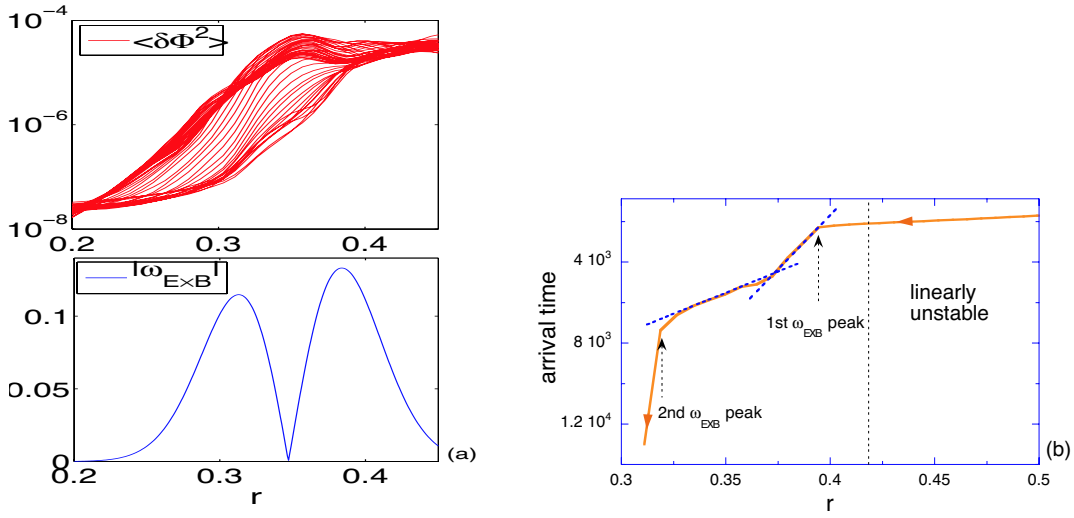

FIG. 7: (a) The spatio-temporal evolution of the propagation front (upper panel) and the $|\omega_E|$ profile (lower panel), and (b) arrival time of turbulence propagation front at different radii. This is the same simulation with $E_0 = 1$ as in Fig. 5.

which shows that the extent of spreading increases with the intensity and decreases with the linear damping rate, *i.e.*, $\Delta \propto \sqrt{V_s/|\gamma|'}$. Therefore, the results depend on the profiles used. To further understand our simulation results for turbulence propagation through a transport barrier, one may extend the previous calculation by including the damping from the $\mathbf{E} \times \mathbf{B}$ shearing flow. This theoretical work will be reported elsewhere.

IV. NONLINEAR DYNAMICS OF ENERGY CASCADING IN ITG SATURATION PROCESS

In this section, we discuss the saturation mechanism of ITG turbulence by examining the nonlinear dynamics of turbulence energy transfer among different modes in (n, m) space, where n and m are toroidal and poloidal mode numbers, respectively. First we define an average toroidal mode number,[27] weighted by the mode intensity $\delta\Phi^2_{mn}$, as follows:

$$\bar{n} \equiv \frac{\sum\limits_{m,n} n\delta\Phi^2_{mn}}{\sum\limits_{m,n} \delta\Phi^2_{mn}}.$$

Figure 8-a plots the time evolution of the averaged n-number at radial location $r = 0.56$, which is around the maximum of the ITG linear drive. In the linear growth phase, the

averaged toroidal mode number is driven up to $\bar{n} = 64$, which corresponds to the most unstable mode with $k_\theta \rho_i \sim 0.35$. Later on, $\bar{n}$ rapidly dropped by 2/3. It should be mentioned that the k-spectrum down-shift phenomenon has been predicted by theories[28,29] and observed in previous simulations.[30] Here what is interesting is that the down-shift phenomenon is observed to occur right during the turbulence saturation process. This suggests that there exists a strong correlation between ITG saturation and turbulence energy transfer to longer wavelength stable modes. Figure 8-b is a locally enlarged plot. It shows that, after an exponential increase, a big "down-jump" in turbulence intensity immediately follows. This type of time behavior in the ITG driven energy flux (or the thermal conductivity χ_i in many publications) has been commonly observed in previous simulations. Our results indicate that the observed "down-jump" is caused by turbulence energy transfer to longer wavelength stable modes. We further examine energy exchange between different modes, which is shown in Fig. 8-c. At the beginning, the most unstable modes with toroidal mode number $61 \leq n \leq 80$ are driven up to contain most of the energy. During turbulence saturation (in a short time period around $t = 200$), the energy is transfered to longer wavelength (stable) modes with $21 \leq n \leq 40$. The energy exchange between the two groups of modes is evidently demonstrated. On the other hand, the k-spectrum of fluctuations in the linearly stable region is determined by the spreading of the turbulence. Roughly, it is observed that in a well developed global turbulence state, the energy tends to concentrate at around $k_\theta \rho_i \sim 0.2$, with radial dependence introduced by $\rho_i \sim (T_i/m_i)^{1/2}/B$.

An immediate question is how the energy is transfered to lower-n modes. Figure 9 shows the energy cascading process in (n, m) space. In the linear phase, only unstable modes are driven, located in a narrow band around a diagonal line, with $m/n \approx q(r)$ (Fig. 9-a), where q is the safety factor. This illustrates the strongly anisotropic nature of these modes, with $k_\parallel \sim (nq - m)/nqR \ll k_\perp$. During the saturation process, the nonlinear toroidal coupling of two unstable eigenmodes generates a low-n quasimode (Fig. 9-b). At the same time, there is an energy coupling to higher-n modes, as also seen in Fig. 9-b. The energy coupling to higher-n modes, however, is weaker due to the higher intrinsic inertia,[31] and generally higher-n modes ($k_\theta \rho_i \gtrsim 1$) are heavily Landau damped. The quasimodes are generated by the following mode coupling process:

$$(n_1, m_1) + (n_2, m_2) \Rightarrow (n_2 \pm n_1, m_2 \pm m_1),$$

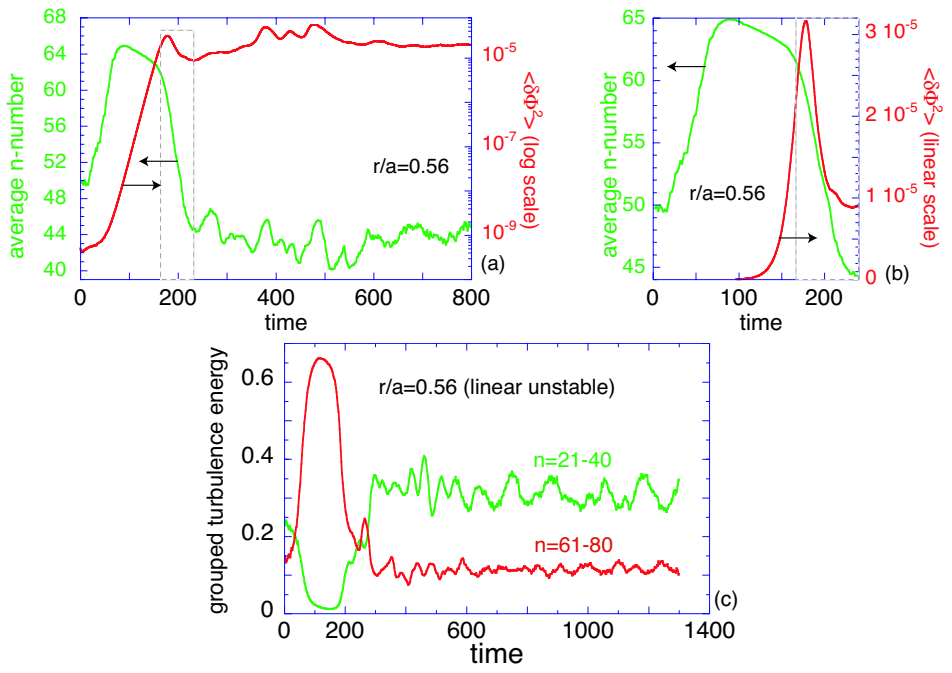

FIG. 8: (a) The time evolution of average toroidal mode number $\bar{n}$ and turbulence intensity $\langle \delta\Phi^2 \rangle$ at $r/a = 0.56$, (b) locally enlarged plot of $\bar{n}$ and $\langle \delta\Phi^2 \rangle$ vs. time with linear scale in $\langle \delta\Phi^2 \rangle$, and c) the time history of energy contained in mode group $21 \leq n \leq 40$ and in group $61 \leq n \leq 80$.

where the pump modes $(n_1,\, m_1)$ and $(n_2,\, m_2)$ are two unstable eigenmodes. It is remarked that this nonlinear interaction causes an energy cascade in (n, m) space nonlocally, resulting in a spectrum gap between the unstable eigenmodes and the quasimodes (Fig. 9-b). At later times, successive nonlinear couplings further transfer energy to fill up the spectrum gap, eventually results in an overall down-shifted spectrum in the fully developed turbulence regime (Fig. 9-c). The later nonlinear process may be dominated by the scattering of unstable eigenmodes (pump modes) off the driven low-n quasimodes,[31] which was observed to be responsible for saturating the electron temperature gradient (ETG) instability in a global gyrokinetic simulation.[32] Another remarkable feature of the k-space nonlinear dynamics is that the turbulence energy cascades toward the low-n modes along the resonance surface $m/n \approx q$. In this respect, linear toroidal mode couplings, which transfer energy among different poloidal harmonics of a single n mode due to the poloidal angle dependence of the magnetic field, may play an important role. This is different than slab geometry simulations in which the particle $\mathbf{E} \times \mathbf{B}$ detrapping process was shown to play an important role in

nonlinear saturation.[33]

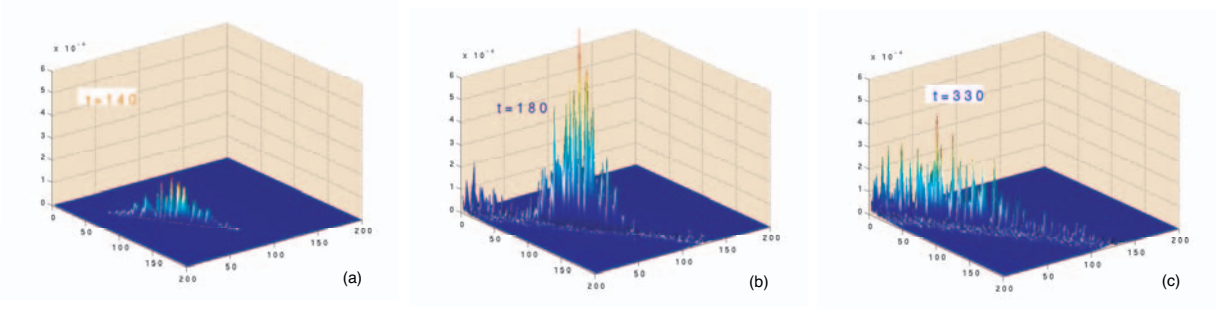

FIG. 9: Three time slices of the fluctuation spectra $\delta\Phi^2_{mn}$ at $r/a = 0.56$: (a) linear growth phase, (b) an earlier time during nonlinear saturation, and (c) fully developed turbulence regime. This is the same simulation as in Fig. 8.

V. DISCUSSION AND CONCLUSIONS

Our global particle simulations using a generalized gyrokinetic model with realistic parameters in shaped plasmas have demonstrated that turbulence spreading is quite a generic phenomenon. The linear spreading due to the linear toroidal mode coupling is convective, which evenly raises, with a constant rate, the radial envelope of fluctuation intensity in the linearly stable region. However, its spreading into the stable region is very limited in both radial extent and intensity. The nonlinear spreading due to the nonlinear wave-wave interactions is shown to be responsible for developing global turbulence, resulting in significant fluctuations (comparable to those in the unstable ITG source region) and enhanced ion energy transport in the linearly stable region. The nonlinear spreading exhibits diffusive, and possibly sub-diffusive, characteristics, being consistent with theories. The major expansion of fluctuations to the stable regions due to nonlinear spreading is observed to occur on a time scale of the order of the linear growth time, right after the nonlinear saturation of the ITG instability. This happens for both turbulence eddies broken by the self-generated zonal flows, and elongated radial streamers as well. The later case corresponds to having the zonal flow generation artificially suppressed in ITG simulations, and corresponds to the observation that there is little zonal flow generation in ETG dynamics. The principal effect of self-generated zonal flows on turbulence spreading observed in our simulations is through

the $\mathbf{E} \times \mathbf{B}$ flow shear induced regulation of turbulence. Compared to the numerical experiments with zonal flow artificially suppressed, both front propagation speed and turbulence extent are reduced in the presence of self-generated zonal flows. This can be accounted for by the fact that zonal flows regulate turbulence intensity to a level usually an order of magnitude lower than that without zonal flows, and the fact that the front propagation speed decreases with the turbulence intensity. It is definitely interesting, but difficult in a simulation, to isolate and identify the nonlinear interactions of drift waves and zonal flows in toroidal plasma as an underlying dynamics for turbulence spreading.

The key results of our simulation study concern the turbulence propagation through a transport barrier, characterized by an $\mathbf{E} \times \mathbf{B}$ shear layer. It has been found that an $\mathbf{E} \times \mathbf{B}$ shear layer with an experimentally relevant level of the shearing rate can significantly reduce, and sometimes even block, turbulence spreading by reducing the spreading extent and speed. The $\mathbf{E} \times \mathbf{B}$ shear blocking is essentially a local process, while turbulence spreading is a nonlocal phenomenon. The key quantity to the control of turbulence spreading is identified to be the local maximum shearing rate $|\omega_E^{max}|$, rather than the amplitude of E_r. The underlying physics may relate to a robust feature of shear flows for turbulence dissipation, which enhances the damping of fluctuations in the shear layer. The role of the equilibrium $\mathbf{E} \times \mathbf{B}$ shear layer as a "barrier" for turbulence spreading revealed by the gyrokinetic simulations, however, represents a new aspect of the transport barrier physics, in addition to the well known quenching effect of shear flow on local instabilities. It may suggest a possible interesting application to the improvement of plasma confinement in experiments. Both experimental observations and computer simulations indicate that the core plasma confinement performance can be degraded by edge turbulence which often has high level fluctuations. Based on the findings from the gyrokinetic simulations, in principle, one may be able to decouple the core plasma from the strongly turbulent edge plasma by creating an $\mathbf{E} \times \mathbf{B}$ shear layer in between, achieving a higher quality of core plasma confinement. Experimental tests of turbulence spreading and control would be highly interesting. Direct tests require measurements of fluctuations inside an internal transport barrier, along with detailed linear stability analysis of a wide k-spectrum range including electromagnetic instabilities. Carefully designed experiments may need to destroy transport barriers (H$\rightarrow$L back transition, enhanced reversed shear back transition, $\cdots$), and to measure spatial-temporal evolution of turbulence recovery, with high resolution measurements of profiles

Finally, our simulation results have demonstrated that the nonlinear toroidal couplings are the dominant k-space activity in ITG saturation dynamics, which cause energy transfer to longer wavelength damped modes, forming a down-shifted toroidal spectrum in the fully developed turbulence regime. The toroidal spectral cascade behavior in ITG dynamics observed in our simulations is qualitatively similar to that found in ETG dynamics,[31,32] although there is stronger zonal flow generation during the saturation process in ITG than in ETG. The self-generated zonal flows in ITG turbulence certainly play an important role in determining the fluctuation level, both locally through a regulating effect (including both shear flow decorrelation and turbulence energy extraction), as well as globally through effects on turbulence spreading. However, the zonal flows are not a necessary component to saturate the turbulence, as the fluctuations can be saturated in the absence of zonal flows. The nonlinear toroidal couplings as a fundamental process appear robust in the drift wave turbulence dynamics of toroidal systems.

Acknowledgments

We acknowledge useful interactions with A. Boozer, L. Chen, P.H. Diamond, X. Garbet, Ph. Ghendrih, O. Gurcan, F.L. Hinton, Y. Idomura, K. Itoh, S.-I. Itoh, Z. Lin, V. Naulin, X. Tang, L. Villard, M. Yagi, and F. Zonca. This work was supported by U.S. DoE Contract No. DE-AC02-76-CHO-3073 and by the U.S. DoE SciDAC Center for Gyrokinetic Particle Simulation of Turbulent Transport in Burning Plasmas.

---

* Electronic address: wwang@pppl.gov

[1] W. X. Wang, G. Rewoldt, W. M. Tang, F. L. Hinton, J. Manickam, L. E. Zakharov, R. B. White, and S. Kaye, Phys. Plasmas **13**, 082501 (2006).

[2] X. Garbet, L. Laurent, A. Samain, and J. Chinardet, Nucl. Fusion **34**, 963 (1994).

[3] Z. Lin, S. Ethier, T.S. Hahm *et al.,* Phys. Rev. Lett. **88**, 195004 (2002).

[4] T. S. Hahm, P.H. Diamond, Z. Lin *et al.*, Plasma Phys. Control. Fusion **46**, A323 (2004).

[5] Z. Lin and T. S. Hahm, Phys. Plasmas **11**, 1099 (2004).

[6] R. E. Waltz and J. Candy, Phys. Plasmas **12**, 072303 (2005).

[7] W. X. Wang, Z. Lin, W. M. Tang, W. W. Lee, S. Ethier, J. L. V. Lewandowski, G. Rewoldt, T.S. Hahm, and J. Manickam, Phys. Plasmas **13**, 092505 (2006).

[8] T. S. Hahm and K. H. Burrell, Phys. Plasmas **2**, 1648 (1995).

[9] R. Waltz *et al.*, Phys. Plasmas **1**, 2229 (1994); G. Rewoldt *et al.*, ibid, **5**, 1815 (1998).

[10] K. H. Burrell, Phys. Plasmas **4**, 1499 (1997); E. J. Synakowski *et al.*, ibid, **4**, 1736 (1997).

[11] R. Nazikian, K. Shinohara, G. J. Kramer *et al.*, Phys. Rev. Lett. **94**, 135002 (2005).

[12] L. Chen, R.B. White, F. Zonca, Phys. Rev. Lett. **92**, 075004 (2004).

[13] T. S. Hahm, P.H. Diamond, Z. Lin *et al.*, Phys. Plasmas **12**, 090903 (2005).

[14] O.D. Gurcan, P.H. Diamond, T.S. Hahm *et al.*, Phys. Plasmas **12**, 032303 (2005).

[15] F. Zonca, L. Chen, and R.B. White, *Theory of Fusion Plasmas*, (Proc. Joint Varenna-Lausanne Int. Workshop, Varenna, 2004) (Bologna: SIF) 3.

[16] W. X. Wang, Bull. Am. Phys. Soc. **50**(8), 180 (2005).

[17] O.D. Gurcan, P.H. Diamond, T.S. Hahm *et al.*, Phys. Plasmas **13**, 052306 (2006).

[18] M. Yagi, T. Ueda, S.-I. Itoh *et al.*, Plasma Phys. Control. Fusion **48**, A409 (2006).

[19] V. Naulin *et al.,* Phys. Plasmas **12**, 122306 (2005).

[20] W. Horton, D.-I. Choi, and W.M. Tang, Phys. Fluids **24**, 1077 (1981).

[21] P. H. Diamond and T. S. Hahm, Phys. Plasmas **2**, 3640 (1995).

[22] S.-I. Itoh and K. Itoh, Plasma Phys. Control. Fusion **43**, 1055 (2000).

[23] R.D. Sydora *et al.*, Plasma Phys. Control. Fusion **38**, A281 (1996).

[24] Y. Idomura, M. Wakatani, and S. Tokuda, Phys. Plasmas **7**, 3551 (2000).

[25] L. Villard, S. J. Allfrey, A. Bottino *et al.*, Nucl. Fusion **44**, 172 (2004).

[26] S.E. Parker *et al.,* Phys. Plasmas **3**, 1959 (1996).

[27] L. Chen, private communication.

[28] P. L. Similon and P. H. Diamond, Phys. Fluids **27**, 916 (1984).

[29] T. S. Hahm and W. M. Tang, Phys. Fluids **B3**, 989 (1991).

[30] S. E. Parker *et al.*, Phys. Rev. Lett. **71**, 2042 (1993).

[31] L. Chen, F. Zonca, and Z. Lin, Plasma Phys. Control. Fusion **47**, B71 (2005).

[32] Z. Lin, L. Chen, and F. Zonca, Phys. Plasmas **12**, 056125 (2005).

[33] W. W. Lee and W. M. Tang, Phys. Fluids **31**, 612 (1988).

The Princeton Plasma Physics Laboratory is operated
by Princeton University under contract
with the U.S. Department of Energy.

Information Services
Princeton Plasma Physics Laboratory
P.O. Box 451
Princeton, NJ 08543

Phone: 609-243-2750
Fax: 609-243-2751
e-mail: pppl_info@pppl.gov
Internet Address: http://www.pppl.gov